



The Generation of Upward-Propagating Whistler Mode Waves by Electron Beams in the Jovian Polar Regions

S. S. Elliott, D. A. Gurnett, P. H. Yoon, W. S. Kurth, B. H. Mauk, R. W. Ebert, G. Clark, P. Valek, F. Allegrini, S. J. Bolton, et al.

► To cite this version:

S. S. Elliott, D. A. Gurnett, P. H. Yoon, W. S. Kurth, B. H. Mauk, et al.. The Generation of Upward-Propagating Whistler Mode Waves by Electron Beams in the Jovian Polar Regions. *Journal of Geophysical Research Space Physics*, 2020, 125, 10.1029/2020JA027868 . insu-03673145

HAL Id: insu-03673145

<https://insu.hal.science/insu-03673145>

Submitted on 23 Jun 2022

HAL is a multi-disciplinary open access archive for the deposit and dissemination of scientific research documents, whether they are published or not. The documents may come from teaching and research institutions in France or abroad, or from public or private research centers.

L'archive ouverte pluridisciplinaire **HAL**, est destinée au dépôt et à la diffusion de documents scientifiques de niveau recherche, publiés ou non, émanant des établissements d'enseignement et de recherche français ou étrangers, des laboratoires publics ou privés.

Copyright

JGR Space Physics

RESEARCH ARTICLE

10.1029/2020JA027868

Special Section:

Jupiter Midway Through the
Juno Mission

Key Points:

- Upgoing electron beams can generate upward-propagating whistler mode waves over the Jovian polar cap region
- Numerical simulations show the electron beams are unstable and capable of producing the observed whistler mode waves
- Large growth rates are found for Landau ($n = 0$) resonance

Correspondence to:

S. S. Elliott,
sadie-tetrick@uiowa.edu

Citation:


Elliott, S. S., Gurnett, D. A., Yoon, P. H., Kurth, W. S., Mauk, B. H., Ebert, R. W., et al. (2020). The generation of upward-propagating whistler mode waves by electron beams in the Jovian polar regions. *Journal of Geophysical Research: Space Physics*, 125, e2020JA027868. <https://doi.org/10.1029/2020JA027868>

Received 30 JAN 2020

Accepted 13 APR 2020

Accepted article online 15 MAY 2020

The Generation of Upward-Propagating Whistler Mode Waves by Electron Beams in the Jovian Polar Regions

S. S. Elliott¹ , D. A. Gurnett¹ , P. H. Yoon^{2,3,4} , W. S. Kurth¹ , B. H. Mauk⁵ ,
R. W. Ebert⁶ , G. Clark⁵ , P. Valek⁶ , F. Allegrini^{6,7} , S. J. Bolton⁶ , J. D. Menietti¹ ,
P. Louarn⁸ , and A. H. Sulaiman¹ 

¹Department of Physics and Astronomy, University of Iowa, Iowa City, IA, USA, ²Institute of Physical Science and Technology, University of Maryland, College Park, MD, USA, ³School of Space Research, Kyung Hee University, Yongin, South Korea, ⁴Korea Astronomy and Space Science Institute, Daejeon, South Korea, ⁵The Johns Hopkins University Applied Physics Laboratory, Laurel, MD, USA, ⁶Southwest Research Institute, San Antonio, TX, USA, ⁷Department of Physics and Astronomy, University of Texas at San Antonio, San Antonio, TX, USA, ⁸Université de Toulouse, IRAP, CNRS, UPS, Toulouse, France

Abstract Upward-moving energetic electrons with energies of 1 MeV and above were observed over the entire Jovian polar region. The electrons were found to be associated with intense broadband whistler mode waves, similar to terrestrial whistler mode auroral hiss. Upward-propagating whistler mode hiss at Earth is known to be generated by upward-moving, magnetic field-aligned electron beams (from electric field-aligned potentials), by a beam-plasma instability at the Landau resonance. Assuming this process at Jupiter, we present a linear stability analysis, showing the electron distribution functions (based on inverted-V observations made by the Juno Jovian Auroral Distributions Experiment, JADE-E, instrument) are unstable. The polarization of the modeled waves is consistent with whistler mode hiss (right-hand circularly polarized). From the results of the linear stability analysis, we find that the calculated growth rates are sufficient to produce the observed whistler mode waves.

1. Introduction

The Juno spacecraft is equipped with instruments that make observations that enable better understanding of the wave-particle interactions that occur at Jupiter. These interactions can provide a mechanism for accelerating charged particles, which can aid in our understanding of the Jovian polar and auroral environment. Two exciting early discoveries made by Juno were observations of upward-traveling energetic electrons (from hundreds of eV to several MeV) and upward-propagating whistler mode waves, occurring simultaneously over the entire polar cap region (Allegrini et al., 2017; Connerney, Adriani, et al., 2017; Mauk, Haggerty, Paranicas, Clark, Kollmann, Rymer, Mitchell, et al., 2017; Tetrick et al., 2017). The waves and electrons were found to be positively correlated (Tetrick et al., 2017), and due to inconsistencies with the first adiabatic invariant motion of the electrons, it was shown that the waves perturb the electron motion and contribute to pitch angle scattering, indicative of significant wave-particle interactions (Elliott, Gurnett, Kurth, Clark, et al., 2018). The whistler mode waves are similar to terrestrial auroral hiss, which is a broadband plasma wave that propagates in the whistler mode and is typically found in the high-latitude auroral regions of planetary magnetospheres. The emission is known to be produced by electron beams via a beam-plasma instability at the Landau resonance velocity, $v_{||} = \omega/k_{||}$ (Gurnett et al., 1986; Maggs, 1976).

For a Landau resonance to occur, the electron beam must move in the same direction as the wave, that is, upward-propagating auroral hiss is generated by upward-traveling electron beams. Due to this condition, Elliott, Gurnett, Kurth, Mauk, et al. (2018) proposed a mechanism to explain the generation of the upward-propagating whistler mode waves and ultimately the acceleration of upward-traveling electrons over the Jovian polar cap region. As a first step, the authors proposed that downward-directed parallel electric fields (i.e., to produce upward-traveling electron beams), in Jupiter's upper ionosphere, produce intense upward-propagating whistler mode waves via the Landau resonance. This theoretical study noted that computer simulations were necessary to show that the growth of these waves can be explained by the observed electron beams (from inverted-Vs) and show that the generated whistler mode waves could energize electrons stochastically.

In this study, we conduct a linear stability analysis and present computed growth rates using model electron distribution functions, with input parameters from inverted-V observations made by the Juno Jovian Auroral Distributions Experiment (JADE-E) instrument (Ebert et al., 2017; McComas et al., 2017). We explore a range of wave normal angles by using the general expression for the linear temporal growth rate of magnetoionic modes, as derived by Yoon and Ziebell (1995) and Yoon et al. (1996). We present results of the polarization for the model-generated waves, which are consistent with whistler mode auroral hiss (i.e., right-hand circularly polarized). The large positive growth rates show that the electron beams are unstable and capable of producing whistler mode waves.

2. Background

Whistler mode auroral hiss was first discovered by ground-based instruments, through the detection of low-frequency broadband electromagnetic emissions in association with the aurora (Martin et al., 1960). Since its discovery, whistler mode hiss has been observed at Earth by various satellites (Gurnett & O'Brien, 1964; Gurnett, 1966; Laaspere et al., 1971; McEwen & Barrington, 1967), and also at Jupiter (Farrell et al., 1993; Gurnett et al., 1979; Gurnett et al., 2005; Tetrack et al., 2017) and Saturn (Gurnett et al., 2009; Kopf et al., 2010; Sulaiman, Kurth, Hospodarsky, Averkamp, Persoon, et al., 2018; Sulaiman, Kurth, Hospodarsky, Averkamp, Ye, et al., 2018). Whistler mode waves can only propagate below both the electron cyclotron frequency and the electron plasma frequency, with an upper cutoff at the lower of the two. A common feature of whistler mode auroral hiss is its characteristic funnel shape, observed on a frequency-time spectrogram. The funnel, sometimes called a saucer, arises from wave propagation at wave normal angles near the resonance cone, which causes the raypath to deviate from the magnetic field direction as frequency increases (Gurnett, 1966; James, 1976; Mosier & Gurnett, 1969; Smith, 1969). The radiation originates from electron beams moving in the same direction as the waves (i.e., Landau resonance). Maggs (1976) was the first to explain the generation of whistler mode auroral hiss by a coherent beam-plasma instability at the Landau resonance velocity. Numerous studies, including a statistical study using data from the Fast Auroral SnapshoT Explorer (FAST) (Pfaff et al., 2001), have shown that the majority of auroral hiss emissions are generated in the auroral downward current regions by low-energy upward-moving electron beams (inverted-Vs) accelerated by downward parallel electric fields (Ergun et al., 2003). It should be noted that the inverted-Vs observed by FAST showed that the electrons can be broad in pitch angle but have peaked energy distributions. In contrast, at Jupiter, the electron angular distributions are much more field aligned. Inverted-Vs, when viewed on an energy-time spectrogram, show peak fluxes at an energy that increases from low energies, reaches a maximum energy, and finally decreases (Frank & Ackerson, 1971; Mauk, Haggerty, Paranicas, Clark, Kollmann, Rymer, Bolton, et al., 2017).

The Juno radio and plasma wave (Waves) instrument (Kurth et al., 2017) detected intense upward-propagating broadband whistler mode waves over Jupiter's entire polar cap region (see Figure 8 in Elliott, Gurnett, Kurth, Mauk, et al., 2018). These waves demonstrate characteristic funnel shapes and are analogous to whistler mode auroral hiss. The waves propagate upward (away from the planet) in both the northern and southern polar regions (analyses from Kolmasova et al., 2018, were used to determine the direction of wave propagation). Similarly, the JADE-E sensor (McComas et al., 2017) detected upward-traveling electron beams (inverted-Vs) in the low-altitude regions of the Jovian polar cap (Ebert et al., 2017; see Figure 8 in Elliott, Gurnett, Kurth, Mauk, et al., 2018) as well as upward-traveling electrons over a broad energy range (Mauk, Haggerty, Paranicas, Clark, Kollmann, Rymer, Mitchell, et al., 2017). We believe that electron beams (inverted-Vs) are producing the whistler mode waves via a Landau resonance. This study does not attempt to conduct a nonlinear analysis due to the lack of detailed observations in the wave source regions, but rather, we present a linear stability analysis to show that the electron beam distribution is unstable and likely the source of the observed whistler mode waves.

3. Model Electron Distribution

In order to show that the electron beams are unstable, growth rate calculations must be made. These calculations require an input electron distribution model. In the following analysis, it is convenient to work with the normalized momentum, $u = p/m_e c$. The model electron distribution function used is a combination of a

Maxwellian background (with density n_0) plus a drifting Maxwellian beam (with density n_e). Equation 1 provides the exact bi-Maxwellian that was used:

$$f(u, \mu) = \frac{1 - \delta}{\pi^{3/2} \alpha_0^3} \exp\left(-\frac{u^2}{\alpha_0^2}\right) + \frac{\delta}{\pi^{3/2} \alpha_1^3} \exp\left(-\frac{u^2(1 - \mu^2) + (u\mu - u_0)^2}{\alpha_1^2}\right) \quad (1)$$

with

$$\delta = \frac{n_e}{n_0}, \quad (2)$$

where $\mu = u_{\parallel}/u$ is the cosine of the pitch angle; n_e and n_0 are the number densities of the energetic electron beam and total background electrons, respectively; and α_0 is the energy of the cold, background electrons. The thermal spread associated with the energetic beaming electrons (electron beam temperature) is α_1 , and u_0 is the average drift speed of the beam normalized to the speed of light.

To model the electron distribution, input parameters such as the beam-to-background density ratio, electron-to-plasma frequency ratio, and the average drift speed are necessary (see Table 1 for a list of the parameters used in the present analysis). Figure 1 shows upward-moving electron beam velocity distribution functions (v_{\perp} vs. v_{\parallel}) for two beams observed on 27 March 2017 (Figure 1a) and on 11 July 2017 (Figure 1b). The beams can be identified in Figure 1 by their enhancements in the phase space density along the negative x axis. Both beams are in the antiparallel direction, where the beam energies are calculated to be about 6.7 and 20 keV, respectively. These beam energies were used to calculate the drift velocities for the two beams. It should be noted that some higher-energy (30 keV) upward-moving beams have been observed by JADE (Ebert et al., 2017) but they are much less intense and are therefore excluded from the current study.

Another important parameter of the electron beam is its number density relative to the background cold plasma density. The electron beam distributions can be integrated over the range of phase space in which the beams exist and then compared to the cold plasma background density. Figure 2 shows plots for the 6.7 keV electron beam on 27 March 2017 (left) and the 30 keV electron beam on 11 July 2017 (right). Figure 2a shows the energy spectra (count and distribution). Figure 2b shows the pitch angle, which is nearly 180° for both beams, meaning the electrons are traveling upward, away from the planet in the southern polar region. Figure 2c shows the total plasma density (from 0.1 to 100 keV), and Figure 2d shows the electron beam density integrated from 5 to 20 keV. Over the duration of the inverted-Vs, the ratios of beam-to-background plasma density range from about 0.1 to 0.4 in both cases, which are very large ratios (strong beams). However, because JADE only measures electrons down to 100 eV during those times, it does not account for lower-energy electrons (colder plasma) in its estimate of the electron density. Thus, we analyzed the total plasma density computed from electron plasma frequency measurements, made by the Waves instrument, based on the upper frequency cutoff of the hiss (see Tetrick et al., 2017). Using the total number densities measured by Waves, the ratios of beam density to cold background, δ , at the times of the selected beams (see Figure 1), reduce to roughly 0.02 (for 27 March 2017) and 0.04 (for 11 July 2017).

Lastly, the ratio between the electron plasma frequency and electron cyclotron frequency, α , is required. The electron cyclotron frequency was determined by the Magnetometer instrument (MAG) by utilizing a pair of triaxial Fluxgate Magnetometers (FGMs) to provide magnetic field measurements at rates up to 64 vector samples/s (Connerney, Benn, et al., 2017). The electron plasma frequency was determined based on the upper cutoff of the whistler mode waves (see Tetrick et al., 2017). These frequency ratios were calculated to be roughly 0.1 (for 27 March 2017) and 0.04 (for 11 July 2017) (see Table 1 for a full list of the parameters used in this study).

4. Growth Rates of the Whistler Mode

The growth rate equation is obtained by analyzing the cold plasma (or magnetoionic) dispersion relation, which is well known and can be found in many plasma physics textbooks (see Gurnett & Bhattacharjee, 2017; Melrose, 1986; Stix, 1962). A complete analysis of the cold plasma dispersion relation and separation of all possible wave modes can be found in Appendix A.

Table 1
List of Plasma Parameters Used in This Study

	27 March 2017, 10:05:55.837 UT	11 July 2017, 03:05:37.501 UT
Electron plasma-to-cyclotron frequency ratio (ω_p/Ω)	0.04	0.04
Electron plasma frequency (ω_p)	$\sim 4.4 \times 10^4$ Hz	$\sim 5.1 \times 10^4$ Hz
Electron cyclotron frequency (Ω)	$\sim 1.1 \times 10^6$ Hz	$\sim 1.4 \times 10^6$ Hz
Energy of beam and associated average drift speed ($\frac{V}{c} = u_0$)	$u_0 = 0.162$ (6.7 keV beam energy)	$u_0 = 0.35$ (20 keV beam energy)
Energy of cold background electrons ($\frac{v_{T0}}{c} = \alpha_0$)	$\alpha_0 = 0.0043$ (10 eV cold background)	$\alpha_0 = 0.0043$ (10 eV cold background)
Thermal spread associated with the energetic beaming electrons ($\frac{v_{Te}}{c} = \alpha_1$)	$\alpha_1 = 0.1$ (5 keV thermal spread)	$\alpha_1 = 0.1$ (5 keV thermal spread)

When computing the linear, temporal growth rate for waves propagating in a collisionless, homogeneous, magnetized plasma, we utilize the weakly relativistic approximation, meaning that the Lorentz factor, $\gamma = (1 + p^2/m^2c^2)^{1/2}$, is replaced by 1 except in the resonance condition, where it is replaced by the delta-function resonance with $\gamma = 1 + p^2/2m^2c^2$. Following the same steps taken by Yoon et al. (1996) and the general expression for the growth rate and notation in the paper by Yoon and Ziebell (1995), the growth rate equation for the whistler mode (Landau resonance) is therefore the following:

$$\gamma = \frac{\omega_p^2 \pi^2}{\omega \omega_{R0}} \Theta(1 - \mu_0^2) \int_{\mu_0}^1 d\mu \sum_{+,-} Q(u_{\pm}, \mu). \quad (3)$$

See Appendix B for a full list of all intermediate variables in Equation 3. The growth rates are calculated numerically with the technique described in Yoon and Ziebell (1995), which yields a solution to the dispersion relation and computed growth rate values. The numerical growth rate calculation results, using Equations 3 and 1, with parameters from Table 1, are shown in the next set of figures.

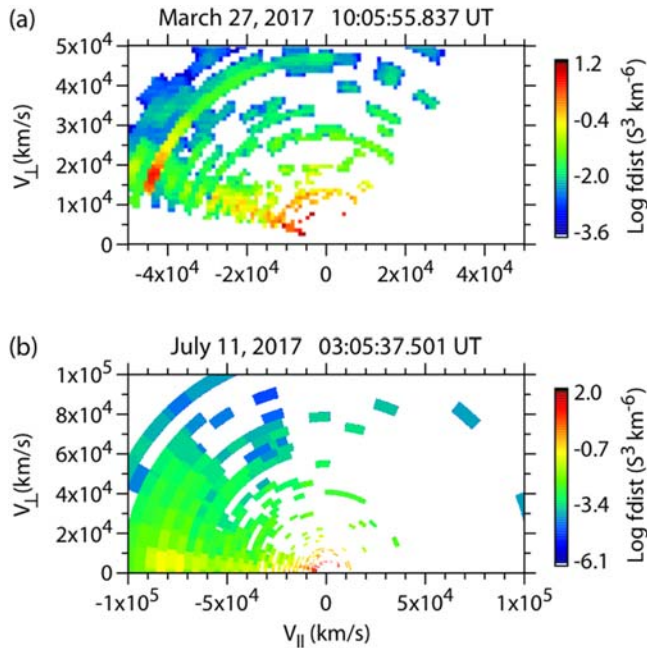


Figure 1. Electron beam velocity distribution plots (v_{\perp} vs. v_{\parallel}) for beams observed on (a) 27 March 2017 and (b) 11 July 2017. The beams are recognized by the enhancement in the antiparallel direction. The energies of the beams are roughly (a) 6.7 keV and (b) 20 keV, which are determined by $E = \frac{1}{2} m_e v^2$, with $v = \sqrt{v_{\perp}^2 + v_{\parallel}^2}$ and the mass of the electron, m_e .

Figures 3 and 4 show the computed growth rates for the two beams. Figure 3 shows the growth rate superposed on the dispersion surface, and Figure 4 shows the 2-D plot in k_{\perp} - k_{\parallel} space. It should be noted that Figures 3 and 4 only include the contributions from $n = 0$ Landau resonance. The cyclotron resonance contribution to the overall growth rate was found to be negligible (on the order of 10^{-31} , for the total, including $n = 0$ and $n = 1$, plots). The large, positive growth rates that were computed demonstrate that the electron beams are unstable and capable of producing waves through a Landau resonance. It should be noted that the dispersion surfaces shown in Figure 3 are actually made of the whistler mode branch, which becomes plasma oscillations with $\omega = \omega_p$ for $\theta \rightarrow 0$. Since this limit is virtually the same as the Langmuir mode, the beam-plasma instability governed by Landau resonance is operative. The cyclotron resonance for quasi-parallel propagation will affect the electron cyclotron mode with frequency $\omega = \Omega$, but for the choice of $\omega_p/\Omega = 0.04$, the electron cyclotron mode becomes part of the Z mode, which is stable.

It was theoretically predicted that whistler mode auroral hiss emissions are right-hand polarized with respect to the local magnetic field (see discussion in Shepherd et al., 1997). Both ground- and space-based polarization measurements of auroral hiss have supported this theory, showing that the wave rotates in the right-hand direction around the magnetic field (Benson & Calvert, 1979; Gurnett et al., 1983; Gurnett & Green, 1978; Harang &

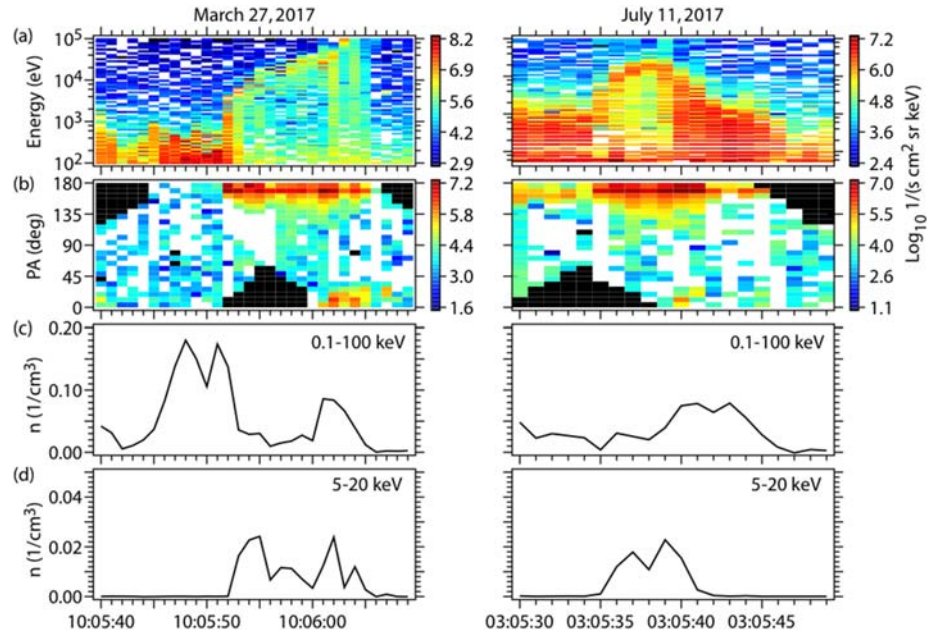


Figure 2. Electron beams on 27 March 2017 (left column) and 11 July 2017 (right column). (a) Energy spectra and (b) pitch angle, with 180° meaning the beam is traveling upward, away from the planet (black regions indicate pitch angles there were not sampled). (c) Total electron density and (d) density of the electron beam, integrated from 5 to 20 keV. Note that the total background density used in our calculations was extracted from measurements of the electron plasma frequency by the Waves instrument.

Hauge, 1965). We define the circular polarization and longitudinal components of the electric field in the same way as Kennel and Wong (1967) (see Appendix C for a complete description of the polarization coefficients). Because the waves produced by the inverted-Vs (via the Landau resonance) are expected to propagate in the whistler mode (similar to auroral hiss), we would expect them to be right-hand circularly polarized. Figure 5 shows polarization plots for varying frequency and wave normal angles. The top panel represents the right-hand circular polarization with respect to the magnetic field direction, where $|e_R| = 1$ indicates right-hand circularly polarized waves. The bottom panel shows the longitudinal electric field component, where $|e_{||}| = 1$ indicates longitudinal waves. Full computation of the polarization coefficients used to generate Figure 5 can be found in Appendix C. We find the whistler mode waves are largely transverse and right-hand circularly polarized, as expected for whistler mode auroral hiss. For more oblique wave propagation, the mode becomes increasingly longitudinal.

Now that we have shown the electron beams are unstable (indicative of high, positive growth rates); it is important to discuss where the observations and numerical results fit together. Although we have calculated

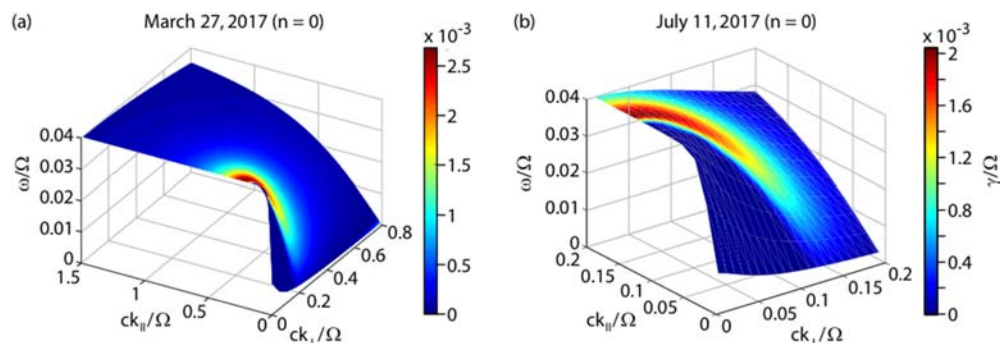


Figure 3. Color-coded computed growth rates for beam parameters that describe the observed beam on 27 March 2017 (a) and 11 July 2017 (b). The growth rate (color) is superposed on the dispersion surface, which depends on frequency and k-space.

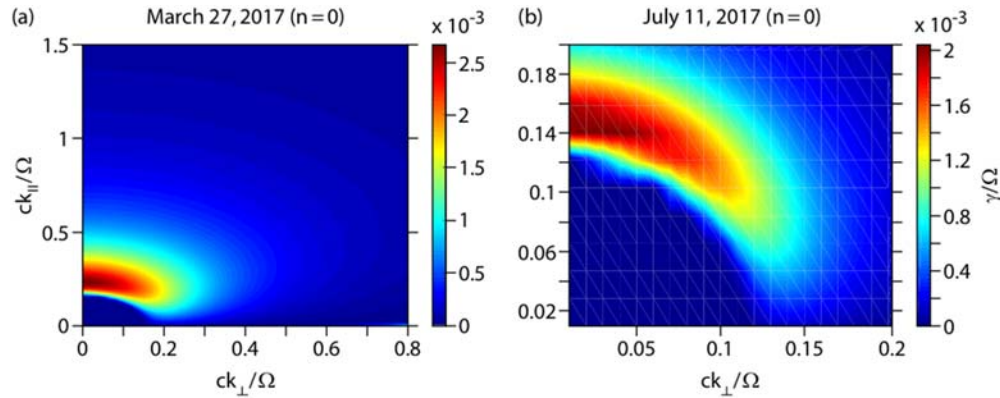


Figure 4. Color-coded computed growth rates for beam parameters that describe the observed beam on 27 March 2017 (a) and 11 July 2017 (b). The growth rate (color) is plotted as a function of k -space.

the growth rates for the whistler mode waves, these numbers are overestimates because they do not take into account nonlinear effects that work to stabilize the distribution function, hence reducing the wave growth rates. An example of nonlinear structures are solitary waves. Figure 6 shows examples of solitary wave structures observed in the whistler mode waveforms for the 2 days of interest in this study. These solitary wave structures (called electrostatic solitary waves or ESWs) are commonly observed in Earth's magnetosphere (e.g., Ergun et al., 1998; Mozer et al., 1997; Temerin et al., 1982). ESWs are known to be the final state of the nonlinear evolution of an electron beam instability (Matsumoto et al., 1994). The observed ESWs could be acting to stabilize the distribution function and would therefore need to be included in future nonlinear simulation studies.

The main takeaway from this study is that we obtain significantly positive growth rates (i.e., well above the state of marginal stability), showing that the electron beams are capable of producing the observed whistler mode waves for even very small background intensities. A similar linear stability analysis was done on whistler mode hiss emissions at Saturn (Kopf et al., 2010). Kopf et al. (2010) studied simultaneously occurring electron beams and whistler mode hiss and found growth rates far above what was needed to produce the observed wave intensities. In some cases, their growth rates were large enough to violate the weak beam approximation.

To provide some logical closure to this study, we have included the observations of the whistler mode waves, which we conclude to be generated by the observed electron beams. Figure 7 shows frequency-time spectrograms for the whistler mode waves over the entire polar regions. These waves possess the same

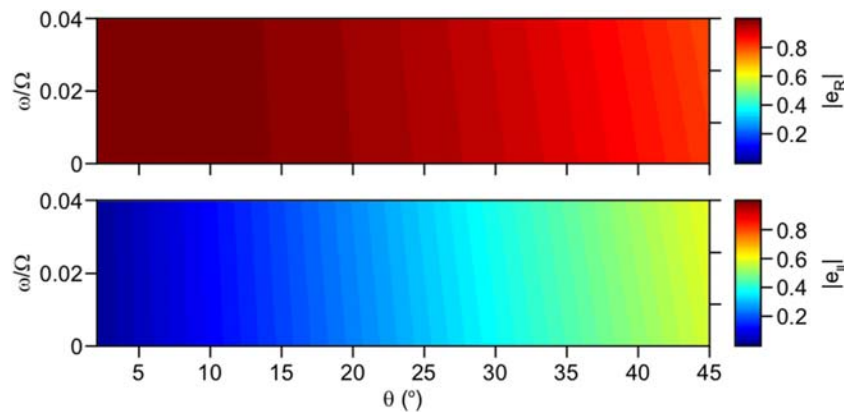


Figure 5. Polarization plots for varying frequency and wave normal angles. Top panel shows the right-hand circular polarization (where $|e_R| = 1$ indicates right-hand circularly polarized waves); bottom panel shows the longitudinal electric field component (where $|e_{\parallel}| = 1$ indicates longitudinal waves). The whistler mode waves are largely transverse, right-hand circularly polarized. Definitions for the polarization coefficients can be found in Appendix C.

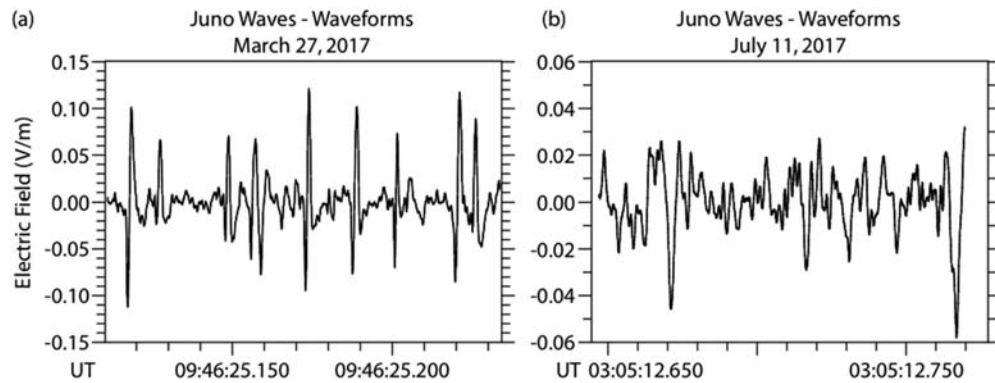


Figure 6. Juno Waves electric field waveforms. The waves show signatures similar to electrostatic solitary waves (ESWs). The irregularity in the electric field suggests nonlinear effects and possible stochastic electron acceleration (see Elliott, Gurnett, Kurth, Mauk, et al., 2018). Please note that the time period for 27 March 2017 waveforms is before the time of the observed electron beam. This is because there are no burst mode measurements during that time period. However, these ESW-like structures are commonly observed over the polar regions.

characteristics as those described in Tetrick et al. (2017); Elliott, Gurnett, Kurth, Clark, et al. (2018); and Elliott, Gurnett, Kurth, Mauk, et al. (2018).

5. Summary and Perspective

In this paper, we have explained the generation of upward-propagating whistler mode waves, in the Jovian polar cap region, by upward-traveling electron beams via Landau resonance. We provided growth rate calculations using model distribution functions based on inverted-V observations from the Juno JADE instrument. We analyzed the polarization of the generated wave and found that the waves are right-hand circularly polarized, as expected for whistler mode auroral hiss. We showed that the growth rates are well above what is needed to produce the observed whistler mode waves. The derived growth rates are overestimates because our study did not take nonlinear effects into account when calculating the values. We provided evidence of nonlinear effects in the whistler mode waves via solitary structures. Therefore, it is likely that these effects are stabilizing the distribution function, ultimately affecting the wave growth rate. Because of this, nonlinear studies would be necessary to fully explain the time evolution of the whistler mode waves and the wave-particle interactions occurring. These nonlinear studies would require more detailed measurements of the wave source region, which are currently unavailable at the time. We leave such analyses for future studies.

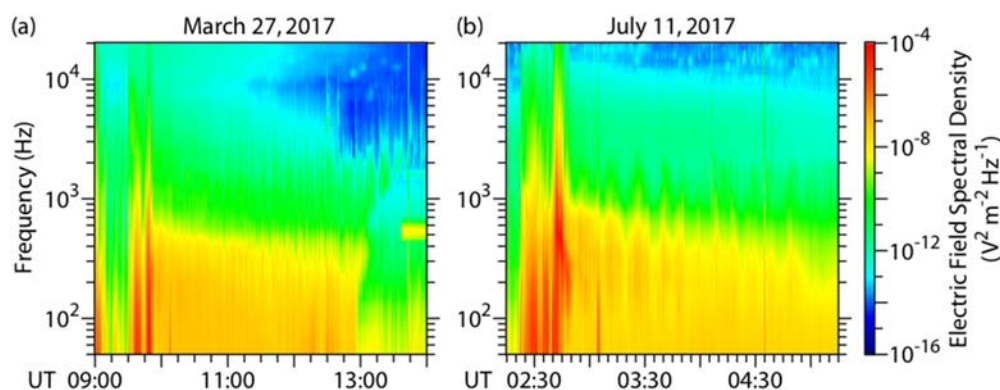


Figure 7. Electric field whistler mode wave observations taken from the Juno Waves instrument over the Jovian polar regions. The whistler mode waves are observed over a broad frequency range, up to the assumed plasma frequency, which is $\sim 4.4 \times 10^4$ Hz for 27 March 2017 and $\sim 5.1 \times 10^4$ Hz for 11 July 2017. The wave emissions for 27 March 2017 begin at $\sim 09:30$ UT and last until $\sim 13:00$ UT. The wave emissions for 11 July 2017 begin at $\sim 02:20$ UT and continue beyond the time period shown, until $\sim 09:30$ UT.

Additional data would be beneficial to these future studies. During the present mission, Juno will directly sample the wave acceleration regions, with a possibility of reaching less than $1.3 R_J$ Jovicentric distance during an extended mission. In these regions, the probability of observing inverted-Vs would likely increase, and we would obtain a better understanding about the plasma environment in the whistler mode wave source region. This opportunity would also provide us with better estimate for the electron distributions by analyzing their time evolution.

Appendix A: Cold Plasma Dispersion Relation

The following equations specify the cold plasma dispersion relation:

$$N^2 = 1 - \frac{T\omega_p^2}{\omega(T\omega - \Omega \cos \theta)}, \quad (\text{A1})$$

where

$$T = \frac{\omega_p^2 - \omega^2}{\omega_p^2 - \omega^2} \left[s - \sigma(1+s^2)^{\frac{1}{2}} \right] \quad (\text{A2})$$

and

$$s = \frac{\omega \Omega \sin^2 \theta}{2|\omega^2 - \omega_p^2| \cos \theta}, \quad (\text{A3})$$

where the modes are separated into the extraordinary (X) and ordinary (O) modes, with $\sigma = +1$ for the X mode and $\sigma = -1$ for the O mode. N in Equation 3 is the index of refraction, where $N = ck/\omega$; Ω is the electron cyclotron frequency, where $\Omega = eB_0/mc$, with the charge of the electron, e ; mass of the electron, m ; and the speed of light, c . The square of the electron plasma frequency, using n_0 as the background number density of electrons, is also defined as $\omega_p^2 = 4\pi n_0 e^2 / m$. The following is the cold plasma dispersion relation separated into the X and O modes:

$$N_X^2 = 1 - \frac{\omega_p^2}{\omega(\omega + \tau \Omega)}, \quad (\text{A4})$$

$$N_O^2 = 1 - \frac{\tau \omega_p^2}{\omega(\tau \omega - \Omega \cos^2 \theta)}, \quad (\text{A5})$$

with

$$\tau = \left(s + \sqrt{s^2 + \cos^2 \theta} \right) \frac{\omega_p^2 - \omega^2}{\omega_p^2 - \omega^2} \quad (\text{A6})$$

and

$$s = \frac{\omega \Omega \sin^2 \theta}{2|\omega^2 - \omega_p^2|}, \quad (\text{A7})$$

which are further separated by frequency ranges into slow and fast modes. The X mode separates into X (fast X) and Z (slow X) modes, and the O mode separates into O (fast O) and W (slow O) modes, according to the frequency ranges defined in Yoon and Ziebell (1995). The present study deals with only the whistler (W) mode.

Appendix B: Intermediate Variables Used in Equation 3

The following defines the function and intermediate variables used in the growth rate equation (Equation 3):

$$Q(u_{\pm}, \mu) = \frac{\cos \theta}{\tau^2 + \cos^2 \theta} \frac{2N_O u_{\pm}^3}{|u_{\pm} - N_O \mu \cos \theta|} \times \left| (K_O \cos^2 \theta + \tau \sin \theta) \mu J_0(b_{\pm}) - (1 - \mu^2)^{\frac{1}{2}} \cos \theta J_1(b_{\pm}) \right|^2 \times \left(\mu u_{\pm} \frac{\partial}{\partial u_{\pm}} + (1 - \mu^2) \frac{\partial}{\partial \mu} \right) f(u, \mu), \quad (B1)$$

with the following parameters defined as

$$K_O = \frac{\omega_p^2}{\omega_p^2 - \omega^2 \tau \omega - \Omega \cos^2 \theta} \tau \Omega \sin \theta \quad (B2)$$

$$R_O = 1 + \frac{\omega_p^2 \cot^2 \theta (\tau^2 \omega_p^2 - \omega^2 \cos^2 \theta) \tau^2 - \cos^2 \theta}{\omega^2 (\tau \omega - \Omega \cos^2 \theta)^2} \frac{\tau^2 + \cos^2 \theta}{\tau^2 + \cos^2 \theta} \quad (B3)$$

$$u_{\pm} = N_O \mu \cos \theta \pm \sqrt{N_O^2 \mu^2 \cos^2 \theta - 2}, \quad (B4)$$

$$\mu_s = \frac{\sqrt{2}}{N_O \cos \theta} \left(1 - \frac{s \Omega}{\omega} \right)^{\frac{1}{2}}, \quad (B5)$$

$$b_{\pm} = \frac{\omega}{\Omega} N_O \sin \theta u_{\pm} (1 - \mu^2)^{\frac{1}{2}}, \quad (B6)$$

where J_s is the Bessel function of the first kind, of order s . For a more detailed derivation of the whistler mode growth rate, see Yoon and Ziebell (1995) and Yoon et al. (1996).

Appendix C: Computation of the Polarization Coefficients

The following provides computation of the polarization coefficients used to generate Figure 5:

The unit electric field vector is given by

$$\hat{\mathbf{e}}(\mathbf{k}) = \frac{K \hat{\mathbf{k}} + T \hat{\mathbf{t}} + i \hat{\mathbf{a}}}{(K^2 + T^2 + 1)^{\frac{1}{2}}},$$

where

$$\begin{aligned} \hat{\mathbf{k}} &= (\sin \theta, 0, \cos \theta) \\ \hat{\mathbf{a}} &= (0, 1, 0) \\ \hat{\mathbf{t}} &= (\cos \theta, 0, -\sin \theta). \end{aligned} \quad (C1)$$

The following properties are true for the longitudinal and transverse modes:

$$\begin{aligned} K &= \infty \text{ (longitudinal mode)} \\ K &= 0 \text{ (transverse mode)} \\ K &= \text{finite and } T = \infty \text{ (transverse mode)}. \end{aligned} \quad (C2)$$

For the whistler mode, K and T are given by the following:

$$K = \frac{\omega_p^2}{\omega_p^2 - \omega^2 \tau \omega - \Omega \cos^2 \theta} \tau \Omega \sin \theta, \quad T = -\frac{\tau}{\cos \theta}. \quad (C3)$$

Therefore, the two transverse electric field components (dimensionless) are given by the following:

$$\hat{e}_{\perp 1} = \frac{T}{(K^2 + T^2 + 1)^{\frac{1}{2}}}, \hat{e}_{\perp 2} = \frac{1}{(K^2 + T^2 + 1)^{\frac{1}{2}}}. \quad (C4)$$

The longitudinal electric field component is given by the following:

$$\hat{e}_{\parallel} = \frac{K}{(K^2 + T^2 + 1)^{\frac{1}{2}}}. \quad (C5)$$

Finally, the right- and left-hand circular polarization can be determined by the following:

$$\hat{e}_R = \frac{\hat{e}_{\perp 1} + \hat{e}_{\perp 2}}{\sqrt{2}}, \hat{e}_L = \frac{\hat{e}_{\perp 1} - \hat{e}_{\perp 2}}{\sqrt{2}}. \quad (C6)$$

Data Availability Statement

Juno data are regularly made publicly available via the Planetary Data System (PDS) according to the Juno Project archiving schedule. More recent data that have not yet been released via the PDS may be requested from the authors.

Acknowledgments

The research at the University of Iowa was supported by NASA through Contract 699041X with the Southwest Research Institute (SwRI). The work at SwRI was funded by the NASA New Frontiers Program for Juno. The JADE data presented here—The JNO-J/SW-JAD-3-CALIBRATED-V2.0 (Version 02 files) and JNO-J/SW-JAD-2-UNCALIBRATED-V1.0 (Version 01 files)—resides at NASA's Planetary Data System (<https://pds.nasa.gov/>). P. H. Y. acknowledges support from GFT Charity, Inc., to the University of Maryland, College Park, BK21 Plus program from NRF, South Korea, to Kyung Hee University, South Korea, and KASI basic research funds. We thank Andrew J. Kopf for his helpful feedback and suggestions, and we also thank Jeremy Faden and Chris Piker for their aid in data acquisition and plotting.

References

- Allegrini, F., Bagenal, F., Bolton, S., Connerney, J., Clark, G., Ebert, R. W., et al. (2017). Electron beams and loss cones in the auroral regions of Jupiter. *Geophysical Research Letters*, 44, 7131–7139. <https://doi.org/10.1002/2017GL073180>
- Benson, R. F., & Calvert, W. (1979). ISIS-1 observations at the source of auroral kilometric radiation. *Geophysical Research Letters*, 6(6), 479–482. <https://doi.org/10.1029/GL006i006p00479>
- Connerney, J. E. P., Adriani, A., Bagenal, F., Bolton, S. J., Cowley, S., Gerard, J.-C., et al. (2017). Jupiter's magnetosphere and aurora observed by the Juno spacecraft during its first polar pass. *Science*, 356(6340), 826–832. <https://doi.org/10.1126/science.aam5928>
- Connerney, J. E. P., Benn, M., Bjarno, J. B., Denver, T., Espley, J., Jorgensen, J. L., et al. (2017). The Juno magnetic field investigation. *Space Science Reviews*, 213(1–4), 39–138. <https://doi.org/10.1007/s11214-017-0334-z>
- Ebert, R. W., Allegrini, F., Bagenal, F., Bolton, S. J., Connerney, J. E. P., Clark, G., et al. (2017). Spatial distribution and properties of 0.1–100 keV electrons in Jupiter's polar auroral region. *Geophysical Research Letters*, 44, 9199–9207. <https://doi.org/10.1002/2017GL075106>
- Elliott, S. S., Gurnett, D. A., Kurth, W. S., Clark, G., Mauk, B. H., Bolton, S. J., et al. (2018). Pitch angle scattering of up-going electron beams in Jupiter's polar regions by whistler-mode waves. *Geophysical Research Letters*, 45, 2590–2596. <https://doi.org/10.1002/2018GL077312>
- Elliott, S. S., Gurnett, D. A., Kurth, W. S., Mauk, B. H., Ebert, R. W., Clark, G., et al. (2018). The acceleration of electrons to high energies over the Jovian polar cap via whistler-mode wave-particle interactions. *Journal of Geophysical Research: Space Physics*, 123, 7523–7533. <https://doi.org/10.1029/2018JA025797>
- Ergun, R. E., Carlson, C. W., McFadden, J. P., Mozer, F. S., Delory, G. T., Peria, W., et al. (1998). FAST satellite observations of large-amplitude solitary structures. *Geophysical Research Letters*, 25(12), 2041–2044. <https://doi.org/10.1029/98GL00636>
- Ergun, R. E., Carlson, C. W., McFadden, J. P., Strangeway, R. J., Goldman, M. V., & Newman, D. L. (2003). Fast auroral snapshot satellite observations of very low frequency saucers. *Physics of Plasmas*, 10(2), 454–462. <https://doi.org/10.1063/1.1530160>
- Farrell, W. M., MacDowall, R. J., Hess, R. A., Kaiser, M. L., Desch, M. D., & Stone, R. G. (1993). An interpretation of the broadband VLF waves near the Io torus as observed by Ulysses. *Journal of Geophysical Research*, 98(A12), 21,177–21,188. <https://doi.org/10.1029/93JA02591>
- Frank, L. A., & Ackerson, K. L. (1971). Observations of charged particle precipitation into the auroral zone. *Journal of Geophysical Research*, 76(16), 3612–3643. <https://doi.org/10.1029/JA076i016p03612>
- Gurnett, D. A. (1966). A satellite study of VLF hiss. *Journal of Geophysical Research*, 71(23), 5599–5615. <https://doi.org/10.1029/JZ071i023p05599>
- Gurnett, D. A., & Bhattacharjee, A. (2017). *Introduction to plasma physics with space and laboratory applications*. Cambridge, UK: Cambridge University Press.
- Gurnett, D. A., & Green, J. L. (1978). On the polarization and origin of auroral kilometric radiation. *Journal of Geophysical Research*, 83(A2), 689–696. <https://doi.org/10.1029/JA083iA02p00689>
- Gurnett, D. A., Kurth, W. S., Hospodarsky, G. B., Persoon, A. M., Averkamp, T. F., Cecconi, B., et al. (2005). Radio and plasma wave observations at Saturn from Cassini's approach and first orbit. *Science*, 307(5713), 1255–1259. <https://doi.org/10.1126/science.1105356>
- Gurnett, D. A., Kurth, W. S., & Scarf, F. L. (1979). Auroral hiss observed near the Io plasma torus. *Nature*, 280(5725), 767–770. <https://doi.org/10.1038/280767a0>
- Gurnett, D. A., Kurth, W. S., Steinberg, J. T., Banks, P. M., Bush, R. I., & Raitt, W. J. (1986). Whistler-mode radiation from the Spacelab 2 electron beam. *Geophysical Research Letters*, 13(3), 225–228. <https://doi.org/10.1029/GL013i003p00225>
- Gurnett, D. A., & O'Brien, B. J. (1964). High-latitude geophysical studies with satellite Injun 3 5. Very low frequency electromagnetic radiation. *Journal of Geophysical Research*, 69(1), 65–89. <https://doi.org/10.1029/JZ069i001p00065>
- Gurnett, D. A., Persoon, A. M., Groene, J. B., Kopt, A. J., Hospodarsky, G. B., & Kurth, W. S. (2009). A north-south difference in the rotation rate of auroral hiss at Saturn: Comparison to Saturn's kilometric radio emission. *Geophysical Research Letters*, 36, L21108. <https://doi.org/10.1029/2009GL040774>
- Gurnett, D. A., Shawhan, S. D., & Shaw, R. R. (1983). Auroral hiss, Z more radiation, and auroral kilometric radiation in the polar magnetosphere: DE 1 observations. *Journal of Geophysical Research*, 88(A1), 329–340. <https://doi.org/10.1029/JA088iA01p00329>
- Harang, L., & Hauge, K. N. (1965). Radio wave emissions in the VLF-band observed near the auroral zone-II, the physical properties of the emissions. *Journal of Geophysical Research*, 70, 499.

- James, H. G. (1976). VLF saucers. *Journal of Geophysical Research*, 81, 501–514. <https://doi.org/10.1029/JA081i004p00501>
- Kennel, C. F., & Wong, H. V. (1967). Resonant particle instabilities in a uniform magnetic field. *Journal of Plasma Physics*, 1, 81.
- Kolmasova, I., Imai, M., Santolik, O., Kurth, W. S., Hospodarsky, G. B., Gurnett, D. A., et al. (2018). Discovery of rapid whistlers close to Jupiter implying similar lightning rates as on Earth. *Nature Astronomy*, 2, 5. <https://doi.org/10.1038/s41550-018-0442-z>
- Kopf, A. J., Gurnett, D. A., Menietti, J. D., Schippers, P., Arridge, C. S., Hospodarsky, G. B., et al. (2010). Electron beams as the source of whistler-mode auroral hiss at Saturn. *Geophysical Research Letters*, 37, L09102. <https://doi.org/10.1029/2010GL042980>
- Kurth, W. S., Hospodarsky, G. B., Kirchner, D. L., Mokrzycki, B. T., Averkamp, T. F., Robison, W. T., et al. (2017). The Juno Waves investigation. *Space Science Reviews*, 213(1-4), 347–392. <https://doi.org/10.1007/s11214-017-0396-y>
- Laaspere, T., Johnson, W. C., & Sempere, L. S. (1971). Observations of auroral hiss, LHR noise, and other phenomena in the frequency range 20 Hz to 540 kHz on Ogo 6. *Journal of Geophysical Research*, 76, 4477.
- Maggs, J. E. (1976). Coherent generation of VLF hiss. *Journal of Geophysical Research*, 81(10), 1707–1724. <https://doi.org/10.1029/JA081i010p01707>
- Martin, L. H., Helliwell, R. A., & Marks, K. R. (1960). Association between aurorae and very low-frequency hiss observed at Byrd Station, Antarctica. *Nature*, 187(4739), 751–753. <https://doi.org/10.1038/187751a0>
- Matsumoto, H., Kojima, H., Miyake, T., Omura, Y., Okada, M., Nagano, I., & Tsutsui, M. (1994). Electrostatic solitary waves (ESW) in the magnetotail: BEN wave forms observed by Geotail. *Geophysical Research Letters*, 21, 2915–2918.
- Mauk, B. H., Haggerty, D. K., Paranicas, C., Clark, G., Kollmann, P., Rymer, A. M., et al. (2017). Discrete and broadband electron acceleration in Jupiter's powerful aurora. *Nature*, 549(7670), 66–69. <https://doi.org/10.1038/nature23648>
- Mauk, B. H., Haggerty, D. K., Paranicas, C., Clark, G., Kollmann, P., Rymer, A. M., et al. (2017). Juno observations of energetic charged particles over Jupiter's polar regions: Analysis of mono- and bi-directional electron beams. *Geophysical Research Letters*, 44, 4410–4418. <https://doi.org/10.1002/2016GL072286>
- McComas, D. J., Alexander, N., Allegrini, F., Bagenal, F., Beebe, C., Clark, G., et al. (2017). The Jovian Auroral Distributions Experiment (JADE) on the Juno mission to Jupiter. *Space Science Reviews*, 213(1-4), 547–643. <https://doi.org/10.1007/s11214-013-9990-9>
- McEwen, D. J., & Barrington, R. E. (1967). Some characteristics of the lower hybrid resonance noise bands observed by the Alouette 1 satellite. *Canadian Journal of Physics*, 45, 13.
- Melrose, D. (1986). *Instabilities in space and laboratory plasmas*. Cambridge: Cambridge University Press. <https://doi.org/10.1017/CBO9780511564123>
- Mosier, S. R., & Gurnett, D. A. (1969). VLF measurements of the Poynting flux along the geomagnetic field with the Injun 5 satellite. *Journal of Geophysical Research*, 74(24), 5675–5687. <https://doi.org/10.1029/JA074i024p05675>
- Mozer, F. S., Ergun, R., Temerin, M., Cattell, C., Dombeck, J., & Wygant, J. (1997). New features of time domain electric field structures in the auroral acceleration region. *Physical Review Letters*, 79(7), 1281–1284. <https://doi.org/10.1103/PhysRevLett.79.1281>
- Pfaff, R., Carlson, C., Watzin, J., Everett, D., & Gruner, T. (2001). An overview of the Fast Auroral SnapshoT (FAST) satellite. *Space Science Reviews*, 98, 1–32. <https://doi.org/10.1023/A:1013187826070>
- Shepherd, S. G., LaBelle, J., & Trimpi, M. L. (1997). The polarization of auroral radio emissions. *Geophysical Research Letters*, 24(24), 3161–3164. <https://doi.org/10.1029/97GL03160>
- Smith, R. L. (1969). VLF observations of auroral beams as sources of a class of emissions. *Nature*, 224(5217), 351–352. <https://doi.org/10.1038/224351a0>
- Stix, T. H. (1962). *The theory of plasma waves*. New York: McGraw-Hill.
- Sulaiman, A. H., Kurth, W. S., Hospodarsky, G. B., Averkamp, T. F., Persoon, A. M., Menietti, J. D., et al. (2018). Auroral hiss emissions during Cassini's Grand Finale: Diverse electrodynamic interactions between Saturn and its rings. *Geophysical Research Letters*, 45, 6782–6789. <https://doi.org/10.1029/2018GL077875>
- Sulaiman, A. H., Kurth, W. S., Hospodarsky, G. B., Averkamp, T. F., Ye, S.-Y., Menietti, J. D., et al. (2018). Enceladus auroral hiss emissions during Cassini's Grand Finale. *Geophysical Research Letters*, 45, 7347–7353. <https://doi.org/10.1029/2018GL078130>
- Temerin, M., Cerny, K., Lotko, W., & Mozer, F. S. (1982). Observations of double layers and solitary waves in the auroral plasma. *Physical Review Letters*, 48, 1175. <https://doi.org/10.1103/PhysRevLett.48.1175>
- Tetrick, S. S., Gurnett, D. A., Kurth, W. S., Imai, M., Hospodarsky, G. B., Bolton, S. J., et al. (2017). Plasma waves in Jupiter's high latitude regions: Observations from the Juno spacecraft. *Geophysical Research Letters*, 44, 4447–4454. <https://doi.org/10.1002/2017GL073073>
- Yoon, P. H., Weatherwax, A. T., Rosenberg, T. J., & LaBelle, J. (1996). Lower ionospheric cyclotron maser theory: A possible source of $2f_{ce}$ and $3f_{ce}$ auroral radio emissions. *Journal of Geophysical Research*, 101(A12), 27,015–27,025. <https://doi.org/10.1029/96JA02664>
- Yoon, P. H., & Ziebell, L. F. (1995). Quasilinear evolution of cyclotron maser instability. *Physical Review E*, 51, 4908. <https://doi.org/10.1103/PhysRevE.51.4908>